Title

Mesolimbic and mesocortical pathways differentially support fentanyl-context associations

Authors

Annalisa Montemarano[1], Hajra Sohail[1], Laura B. Murdaugh[1], Kyrsten Derr[1], Farrah A. Alkhaleel[1], Logan D. Fox[1], Samiksha Pandey[1], Megan E. Fox[1,2,3]

1. Department of Anesthesiology and Perioperative Medicine, Pennsylvania State University College of Medicine, Hershey PA
2. Department of Neuroscience and Experimental Therapeutics, Pennsylvania State University College of Medicine, Hershey PA
3. Address correspondence to Megan E. Fox

   500 University Drive

   C2850, MC #H187

   Hershey, PA 17033

   Tel:717-531-0003 x289635

   mfox@psu.edu

Abstract

Rationale: Synthetic opioids like fentanyl are contributing to unprecedented overdose rates, yet the neural circuitry underlying fentanyl-associated behaviors remains poorly understood. The ventral tegmental area (VTA) projects to both the nucleus accumbens (NAc) and prefrontal cortex (PFC), forming mesolimbic and mesocortical pathways that are implicated in drug-cue associations, though their specific roles in fentanyl-context encoding are not well defined.

Objectives*:* This study aimed to determine how mesolimbic and mesocortical circuits contribute to fentanyl-context associations, and to assess the role of dopamine receptor signaling within these pathways.

Methods*:* Male and female mice underwent fentanyl conditioned place preference (CPP; 0.2 mg/kg). We locally inhibited dopamine D1 or D2 receptors in NAc or PFC during CPP expression. We used fiber photometry calcium imaging to measure activity in VTA-NAc and VTA-PFC projection neurons, and chemogenetic inhibition to suppress their activity during fentanyl CPP.

Results*:* Fentanyl preference was attenuated by blocking D1 but not D2 receptors in PFC, and D2 but not D1 receptors in NAc. We found both VTA-NAc and VTA-PFC exhibited increased calcium activity in response to fentanyl exposure and during entries to the fentanyl-paired context. We further identified a functional role for VTA-NAc in fentanyl CPP expression, as chemogenetic inhibition of VTA-NAc, but not VTA-PFC, reduced fentanyl preference.

Conclusions: While both mesolimbic and mesocortical pathways are activated during fentanyl CPP, they recruit different downstream dopamine receptors. Further, activity in VTA-NAc functionally supports the expression of fentanyl place preference. Together, these findings indicate that mesolimbic and mesocortical circuits differentially contribute to fentanyl-context associations.

INTRODUCTION

Opioid use disorder (OUD) is a chronic, relapsing condition that impacts millions of individuals. The rate of opioid overdose deaths in the U.S. has dramatically escalated in recent years, primarily due to increased prevalence of potent synthetic opioids like fentanyl (Spencer et al. 2024). Fentanyl possesses unique pharmacological properties compared to other opioids: its high lipid solubility allows for rapid passage through the blood brain barrier (Kelly et al. 2023), it exhibits unique binding interactions with the mu opioid receptor (Sutcliffe et al. 2022), and distinct receptor selectivity as compared to morphine (Eshleman et al. 2020). Fentanyl exposure is associated with poorer treatment outcomes for OUD (Socias et al. 2022; Kawasaki et al. 2026), necessitating novel advances in treatment for OUD cases that involve fentanyl. Despite the increased prevalence of fentanyl misuse, an understanding of the neuroadaptations that underly fentanyl misuse remains lacking.

Advancing OUD treatment requires improving our understanding of how opioid-cue associations are formed, as recognition of drug cues contributes to craving and eventual relapse (Vafaie and Kober 2022). One of the most common preclinical models of drug-cue associations is conditioned place preference (CPP). During CPP, subjects develop drug-context associations over several conditioning sessions, then will preferentially seek out the drug-paired context in the absence of drug. A significant mediator of these processes is the ventral tegmental area (VTA), a heterogenous midbrain structure important for drug reward (Koob and Volkow 2010; Doyle and Mazei-Robison 2021). VTA activity and dopamine release in downstream nucleus accumbens (NAc) and prefrontal cortex (PFC) are closely linked to CPP. VTA calcium activity increases during entries to a cocaine-paired context (Calipari et al. 2017), and VTA inactivation with baclofen and muscimol attenuates cocaine place preference (Shinohara et al. 2017). Extracellular dopamine increases in NAc during entries to a heroin-paired context (O'Neal et al. 2022), and in both NAc and PFC during the expression of cocaine CPP (Kawahara et al. 2021). Dopamine D1 and D2 receptors differentially regulate CPP depending on the conditioned drug. For example, amphetamine CPP is attenuated by either NAc D1 or D2 blockade (Hiroi and White 1991), while neither D1 nor D2 blockade influences nicotine (Spina et al. 2006) or alcohol CPP (Young et al. 2014). Morphine CPP is attenuated by D1 but not D2 blockade in NAc (Shippenberg et al. 1993), however these mechanisms may not extend to the synthetic opioid fentanyl. Indeed, fentanyl vs morphine differentially

alter striatal dopamine metabolism (Finlay et al. 1988), necessitating additional investigation on dopaminergic signaling mechanisms of fentanyl-context associations.

While VTA dopamine contributes to CPP, not all VTA dopamine neurons are functionally identical. Rather, they exhibit several distinct properties depending on whether they project to NAc or PFC, including different baseline electrophysiological (Lammel et al. 2008; Chaudhury et al. 2013; Friedman et al. 2014; Juarez and Han 2016) and molecular (Sesack et al. 1998; Lewis et al. 2001; Lammel et al. 2008) signatures, as well as different responses to opioids (Margolis et al. 2006; Simmons et al. 2019; Morison et al. 2025). As such, VTA dopamine neurons that project to NAc or PFC may also exert differential regulation over opioid-associated behaviors, but this has not been fully characterized *in vivo*. Though VTA terminals in NAc exhibit increased activity in response to cocaine CPP (Calipari et al. 2017), it is unknown if this function extends to mesocortical neurons, or to opioid CPP. Furthermore, dopamine is not critical for opioid-context associations, since dopamine deficient mice (Hnasko et al. 2005) and D1-receptor knockout mice (Ting-A-Kee et al. 2013) can form opioid place preferences. Non-dopamine neurons in VTA may be important for opioid-context associations. Indeed, the VTA contains multiple neuron subtypes capable of releasing glutamate, GABA, or a combination of these (Phillips et al. 2022; Fox et al. 2024; Fitzgerald and Day 2025), and recent work indicates many behavioral functions classically attributed to VTA dopamine neurons can also be mediated by glutamate (Root et al. 2014; Wang et al. 2015; Zell et al. 2020; McGovern et al. 2021), GABA (Tan et al. 2012; van Zessen et al. 2012), and co-transmitting (Yoo et al. 2016; Root et al. 2020; Warlow et al. 2024) neurons. These functions extend to opioid use, as VTA GABA and glutamate neurons express mu opioid receptors (Oriol et al. 2025), participate in opioid seeking behaviors (Bossert et al. 2004; McGovern et al. 2023), and undergo diverse molecular adaptations following fentanyl self-administration (Fox et al. 2024). An understanding of how multiple VTA neuronal subtypes contribute to opioid CPP can improve our understanding of how opioid-context associations are formed.

In this study we sought to understand how mesolimbic and mesocortical pathways differentially promote fentanyl-context associations. Consistent with other drug-context associations, we found blocking D1 but not D2 receptors in PFC attenuated fentanyl CPP. Unlike other drug-context associations, we found blocking D2 but not D1 receptors in NAc attenuated fentanyl CPP. To investigate upstream VTA activity that could mediate these effects, we then targeted VTA neurons that either project to PFC (VTA-PFC) or to NAc

(VTA-NAc) in a cell type-agnostic manner. Using *in vivo* calcium imaging, we found both projections exhibited similar activation during fentanyl CPP. However, chemogenetic inhibition of VTA-NAc, but not VTA-PFC, attenuated fentanyl place preference. These experiments support projection-specific functions for multiple VTA neuron subtypes in fentanyl-context associations, thus providing mechanistic insight into the neural encoding of fentanyl-associated behaviors.

MATERIALS AND METHODS

Experimental subjects

All procedures were approved by the Institutional Animal Care and Use Committee at the Pennsylvania State University College of Medicine (PSUCOM) and conducted in accordance with NIH guidelines for the use of laboratory animals. C57BL/6J and RiboTag mice on a C57BL/6J background were obtained from The Jackson Laboratory (RRID:IMSR_JAX:029977) and bred at PSUCOM. All mice were given food and water *ad libitum* and housed in the PSUCOM vivarium on a 12:12h light:dark cycle with lights on at 7:00. Mice were group housed in corncob bedding and provided with nestlets, or pair-housed across a perforated acrylic divider after fiber optic or infusion cannula implantations to prevent isolation stress. All experiments used mice of both sexes (defined gonadally) aged 8-10 weeks at the start of behavior.

Stereotaxic surgery

Adeno-associated viruses for Cre recombinase (AAVrg.hSyn.HI.eGFP-Cre.WPRE.SV40 or AAV-CMV-PI-Cre), Cre-dependent GCaMP8s (AAV9-syn-FLEX-jGCaMP8s-WPRE), Cre-dependent Gi-coupled (AAV9-hSyn-DIO-hM4D(Gi)-mCherry) Designer Receptors Exclusively Activated by Designer Drugs (DREADDs), and Cre-dependent mCherry control (AAV9-hSyn-DIO-mCherry) were acquired from Addgene (viral preps #105540-AAVrg, 105537-AAV9, 162377-AAV9, 44362-AAV9, 50459-AAV9). Mice were anesthetized with 1-4% isoflurane gas in oxygen delivered at 1 liter/min, and affixed in a stereotaxic frame (Stoelting, Dale IL). Mice had a small burr hole made over target brain regions using the following coordinates (in mm, relative to bregma): NAc core (AP +1.6, ML ±1.5, DV -4.4, 10° angle), PFC (AP +1.7, ML ±0.75, DV -2.5, 15° angle), VTA (AP -3.2, ML ±1.0, DV -4.6, 7° angle). Viral vectors were delivered with Hamilton neurosyringes with 33-gauge needles at a rate of 100 nL/min for a total volume of 300 nL/virus, then needles were left in place for 5 min to minimize spread up the tract. For fiber photometry, AAV-CMV-Cre was infused bilaterally in NAc core or PFC of

wildtype mice, 0.4 nL DIO-GCaMP was infused unilaterally in the right VTA (AP -3.2, ML +0.4, DV -4.2, 0° angle), two screws were fixed to the skull, then a fiber optic cannula (Thorlabs #CFM14L05) was implanted above the right VTA (DV -4.0) and fixed to the skull with C&B Metabond Adhesive Cement (Parkell #S380). For chemogenetic experiments, AAVrg-hSyn-eGFP-Cre was infused bilaterally in NAc core or PFC of wildtype mice, and DIO-hM4Gi or DIO-mCherry was infused bilaterally in VTA. For Riboseq, AAVrg-hSyn-eGFP-Cre was infused bilaterally in NAc core or PFC of Ribotag mice. For intracranial pharmacology, two screws were fixed to the skull, then a bilateral guide cannula targeting PFC (RWD, Sugar Land, TX) was implanted at AP +2.1, ML ±0.3, DV -1.7, or targeting NAc (P1 Technologies, Roanoke, VA) was implanted at AP +1.6, ML ±1.5, DV -4.0. Cannula were fixed to the skull with dental cement (#10-000-786, Stoelting, Wood Dale, IL).

Drugs

Fentanyl citrate (#22659) obtained from Cayman chemical (Ann Arbor, MI), and deschloroclozapine (#7193) obtained from Tocris Bioscience (Minneapolis, MN), were dissolved in sterile saline (0.9%). SCH23390 hydrochloride (#HB1643) obtained from Hello Bio (Princeton, NJ) and raclopride (#17422) obtained from Cayman chemical (Ann Arbor, MI) were dissolved in phosphate buffered saline (PBS).

Conditioned place preference

Conditioned place preference (CPP) was performed as previously described (Montemarano et al. 2025) in a three-chambered rectangular apparatus consisting of a neutral center compartment and two side compartments with different contextual cues, connected by automatic guillotine doors, and equipped with infrared photobeam detectors that track animal position and movement (ENV-3013, MED Associates). On the first day of testing (pre-test), mice underwent a 5 min habituation in the center compartment, after which the doors opened, and they freely explored the entire apparatus for 20 min. The least-preferred chamber was subsequently assigned as the fentanyl-paired chamber. Mice then underwent 3 consecutive days of conditioning. On conditioning days, mice received an i.p. injection of saline (10 mL/kg) and were confined to the saline-paired compartment for 20 min; 4 h later, they received an i.p. injection of fentanyl (0.2 mg/kg) and were confined to the fentanyl-paired compartment for 20 min. On the fifth day of testing (post-test), after 5 min habituation in the center, they freely explored the entire apparatus for 20 min. To ensure mice were exhibiting a robust place preference, for mice to be included in analysis across all experiments, they had to spend more time in the fentanyl-paired context during the post-test vs pre-test, as well as more time in the fentanyl-paired

than the saline-paired context during the post-test. Locomotion was measured as movement counts in Med-PC V Software.

Intracranial pharmacology

At least 3 days after cannula implantation, mice underwent CPP as described above. Prior to the post-test, mice received intracranial infusions of SCH23390 (0.2 ug / 0.5 uL infused over 1 minute) (See 2009) or PBS. Microinjectors targeting PFC extended 0.5 mm below the guide cannula (-2.2 DV) and for NAc extended 0.1 mm below the guide cannula (-4.1 DV). The infusers were left in place for 5 minutes, then mice started the post-test after an additional 5 minutes. This was repeated four hours later with the opposite treatment (mice that received SCH23390 before the first post-test then received PBS before the second post-test, and vice versa). A separate cohort of mice received intracranial infusions of raclopride (1 ug / 0.5 uL infused over 1 minute) (Czachowski et al. 2001) or PBS before the post-test using the same design.

Fiber photometry

Three weeks after surgery, mice were habituated to a dummy headstage in their homecage (2-3 days, ~10 min/day). Changes in GCaMP8s fluorescence were acquired with a TeleFipho Wireless Fiber Photometry system (Amuza, San Diego, CA) and synchronized to behavioral events with TTL pulses via an AD instruments Interface and Lab Chart Lightning software (Colorado Springs, CO). Prior to the first behavioral test, a >10 minute recording was taken to confirm GCaMP expression. A >5 minute recording was taken immediately prior to each CPP session to minimize signal decay during testing. Recordings were taken for pre-test, post-test, and all conditioning sessions (470 nm LED @ ~30uW excitation power; 500-550 nm emission). After testing completed, mice were perfused and brains processed for immunostaining as described below to confirm viral expression and fiber placement. Custom MATLAB scripts were made for processing & analysis of fiber photometry recordings. To process recordings, TTL timestamps were used to trim recordings from start to end and a double exponential fit of the signal was generated as a pseudoisobestic control for debleaching (Sherathiya et al. 2021). $\Delta F/F$ was computed as $(F - F_0)/F_0$, where the baseline fluorescence (F_0) was obtained from a linear fit of the fluorescence signal over the full 20-minute recording(Lerner et al. 2015). The $\Delta F/F$ trace was then z-scored using its mean and standard deviation to generate $z\Delta F/F$. Calcium transients

were identified using the findpeaks function in MATLAB, using the following criteria: (1) peak height ≥3x median absolute deviation, (2) peak width >300ms, and (3) distance from previous peak ≥500ms. Due to recording errors during conditioning sessions, any mice that did not have all 6 conditioning recordings were excluded from analysis of conditioning data (n=5). For test days, we generated 4 second zΔF/F snippets centered around context entries (±2 sec) from the entire session zΔF/F trace (no additional baseline subtraction). Snippets were filtered such that a mouse must have been inside the saline or fentanyl paired context for ≥2 seconds. To control for behavioral differences among mice, only the first 15 filtered transitions into each compartment were included for each mouse, the minimum number observed across mice. To compare peri-transition waveforms, we adapted the MATLAB script developed by Jean-Richard-dit-Bressel and colleagues to obtain bootstrapped 95% confidence intervals (Jean-Richard-dit-Bressel et al. 2020). No mice were excluded during test day recordings (no technical errors).

Chemogenetics

At least 14 days after stereotaxic surgery, mice underwent fentanyl CPP as described above, except mice received i.p. injection of saline (or DCZ) 20 min before the post-test. Four hours later, mice were injected with 0.1 mg/kg DCZ (or saline) 20 min before a second post-test (Montemarano et al. 2025). After testing, mice were euthanized, brains removed, and a stereomicroscope equipped with a fluorescence adapter (NightSea, Hatfield PA) was used to confirm GFP-tagged Cre expression in projection targets and mCherry-tagged hM4Gi expression in VTA. To validate our chemogenetic approach, a separate cohort of mice received the same stereotaxic surgery to express DREADDs in VTA-NAc or VTA-PFC. After surgical recovery and viral expression (≥14d) mice received an i.p. injection of 0.1 mg/kg DCZ to activate DREADDs, then 0.2 mg/kg fentanyl to induce cFos expression 20 min later. Mice were transcardially perfused ~1 hour later to capture fos expression as described below.

Immunostaining

Mice were transcardially perfused with PBS and 4% paraformaldehyde under isoflurane anesthesia. Brains were removed and post-fixed for 24hr, then sectioned to a thickness of 50 µm with a compresstome (Precisionary Instruments, Ashland MA.) Slices from GCaMP brains were washed with PBS and blocked for 30 min in in PBS with 3% normal donkey serum and 0.3% Triton X-100. Slices were incubated at 4ºC overnight in blocking buffer containing appropriate primary antibodies (1:1000 chicken anti-GFP, Aves Lab, Tigard, OR,

#GFP-1020; 1:1000 rabbit anti-tyrosine hydroxylase [TH], Calbiochem #657012). Slices were washed 3x10 min with PBS, then incubated for 2h in PBS containing secondary antibodies (1:500, Goat anti-Chicken FITC, Aves Lab, #F-1005; Donkey anti-Rabbit Alexa Fluor 594, Jackson Immuno, West Grove, PA, #711-585-152). Slices were washed with PBS 3 x 10 min, counterstained with DAPI, mounted with Fluoromount-G (Southern Biotech, Birmingham, AL), and imaged on a laser-scanning confocal (Leica SP8) or epifluorescence microscope (Nikon Labophot2). For DREADDs validation, slices were washed with PBS and blocking buffer as above then incubated overnight in the appropriate primary antibodies (1:1000 chicken anti-GFP, Aves Lab, Tigard, OR, #GFP-1020; 1:1000 guinea pig anti-RFP, Synaptic Systems, Göttingen, Germany, #390 004; 1:1000 rabbit anti-cFos, Synaptic Systems #226 008). Slices were washed 3x10 min with PBS, incubated for 30 minutes in PBS with 0.5% Triton X-100, then NeuroTrace was added (1:100, Invitrogen #N21479) and slices incubated for an additional 60 min. Slices were then washed 2x5 min then 1x2hr in PBS, then incubated for 2h in PBS containing secondary antibodies (1:500, Goat anti-Chicken FITC, Aves Lab, #F-1005; Donkey anti-guinea pig TRITC, Jackson #706-025-148; Donkey anti-Rabbit Alexa Fluor 647, Jackson #711-605-152). Slices were mounted with Fluoromount-G and imaged on a laser-scanning confocal.

Cell counting

A subset of wildtype mice received stereotaxic surgery to express GCaMP in VTA-NAc or VTA-PFC neurons as described above, but did not receive a fiber optic cannula to avoid tissue damage artifacts. After >3 weeks, they were perfused and VTA slices were processed for immunostaining of GFP and TH as described above. Images of the right VTA were acquired using a laser-scanning confocal. Three VTA images were pooled per mouse. TH expression was used to outline VTA boundaries, then two blinded investigators independently counted the number of GCaMP-expressing neurons in VTA and how many co-localized with TH to obtain percentage TH-positive GCaMP neurons in VTA. Both investigators' counts were averaged together to obtain one percentage per image. For cFos validation of DREADDs, images of the entire VTA were acquired using a laser-scanning confocal, pooling 2-4 VTA images per mouse. Boundaries were drawn around the VTA based on landmarks visualized with NeuroTrace, then two investigators independently obtained percentage cFos-positive mCherry neurons in VTA as above.

RNA Isolation & Sequencing

Mice were euthanized by cervical dislocation, and brains were rapidly removed and chilled in ice cold PBS. Cold brains were cut into 1 mm coronal sections using an aluminum brain matrix, and tissue punches containing total VTA were collected with 14-gauge needle, then snap-frozen on dry ice and stored at -80 until processing.

Polyribosomes were immunoprecipitated as described previously (Fox et al. 2020, 2023). Tissue punches from RiboTag mice (3 mice pooled per sample) were homogenized by douncing in 1 mL homogenization buffer, and 50µL supernatant saved as input. Remaining supernatant was incubated with 5 µl anti-HA antibody (BioLegend #901515) at 4ºC overnight with constant rotation. Samples were then incubated with 400 uL of protein A/G magnetic beads (Thermo Scientific #88803) overnight at 4ºC with constant rotation. Beads were washed in a magnetic rack with high-salt buffer. RNA was extracted using Trizol (Invitrogen) and the RNeasy Mini Kit with a DNAse step (Qiagen) from both immunoprecipitated and input samples by adding lysis buffer supplemented with beta mercaptoethanol and following the manufacturer's instructions (3-5 samples/sex/projection, 45 total mice). RNA quality and concentration were assessed using an Agilent BioAnalyzer, and cDNA libraries were prepared by the PSUCOM Genome Sciences Core using the SMARTer Stranded Total RNA-Seq Kit v3 – Pico Input Mammalian (Takara Bio, San Jose, CA) according to the manufacturer's instructions. Libraries were quantified by qPCR prior to sequencing on an Illumina NovaSeq 6000 (50 base pair paired-end reads; average of ~70 million reads per sample). Raw data were demultiplexed using bcl2fastq (Illumina), and adapter trimming was performed after UMI extraction with UMI-tools (Smith et al. 2017). Sequencing reads were aligned to the mouse reference genome (GRCm39, Ensembl release 2.7.1a) using STAR (Dobin et al. 2013) with a maximum of two mismatches allowed per read. Gene-level counts were obtained using featureCounts (Liao et al. 2014), with multi-mapping reads included, reads assigned to multiple overlapping features counted fractionally, and the feature with the largest overlap prioritized. We used limma (lmfit) (Ritchie et al. 2015) in R (v4.5.2) to normalize counts (log2CPM) and determine differential expression between projection neurons vs total VTA with post hoc contrasts (makeContrasts). To asses cell-type enrichment across projections, we used the mean_ratios function from DeconvoBuddies (Huuki-Myers et al. 2025) in conjunction with our previously published snRNAseq dataset of mouse VTA (Fox et al. 2024). The top 50 markers per cluster with a MeanRatio >1 were selected. Overlap between differentially expressed genes and cluster markers was evaluated using Fisher's exact test. For each projection, the proportion of differentially expressed genes

mapping to each marker-defined cell class was calculated as the number of overlapping genes divided by the total number of differentially expressed genes overlapping any cluster marker.

Data analysis

Except where noted, data were analyzed with GraphPad Prism (v10), and were collapsed across sex in the absence of significant sex effects or interactions. For intracranial pharmacology experiments, data were analyzed with paired t-tests. For calcium activity during drug exposure, we only included mice with all 6 conditioning recordings (n=14 out of 19 total mice), and data were analyzed with paired t-tests. For calcium activity during CPP test days, to control for behavioral differences, only the first 15 transitions into each region were analyzed for each mouse, which was the minimum number of transitions observed across all mice. Peri-event signal was analyzed with bootstrapped 95% confidence intervals in MATLAB (Jean-Richard-dit-Bressel et al. 2020), and mean signals within a specific time window (analogous to AUC) were analyzed with paired t-tests. For chemogenetic experiments, data were analyzed with two-way repeated measures ANOVA with factors of virus and agonist, and significant interactions were followed up with Sidak's post hoc.

RESULTS

Fentanyl place preference is attenuated by D1R blockade in PFC but not NAc

Dopaminergic mechanisms regulating drug-context associations vary across misused drugs. It remains unknown which dopamine receptors promote fentanyl-context associations. To address this, we locally blocked D1Rs in PFC or NAc during fentanyl CPP expression. Using a counterbalanced, within-subject design, mice underwent two post-tests 4 hours apart, each preceded by an intracranial infusion of either vehicle or the D1 receptor antagonist SCH23390 (Timeline in **Fig 1A,** cannula placements in **Fig 1B, F**). We found that intra-NAc infusion of SCH23390 had no effect on fentanyl place preference compared to vehicle (**Fig 1C-D**). The absence of behavioral effect was not due to an ineffective dose, as intra-NAc infusion of SCH23390 did reduce locomotion (**Fig 1E;** t_{17}=2.9, p=0.01). In contrast, intra-PFC infusion of SCH23390 reduced time spent in the fentanyl-paired side (**Fig 1G;** t_{17}=2.17, p=0.045) and preference for the fentanyl over saline side (**Fig 1H;** t_{17}=2.35, p=0.031) relative to vehicle. Intra-PFC infusion of SCH23390 did not impact locomotion (**Fig 1I**).

Fentanyl place preference is attenuated by D2R blockade in NAc but not PFC

Given the region-dependent effects of D1 receptor blockade on fentanyl CPP, we next investigated D2 receptors. We administered the D2 receptor antagonist raclopride in either PFC or NAc immediately prior to the post-test (**Fig 2A**). In contrast to the D1R antagonist, intra-NAc infusion of raclopride reduced time spent in the fentanyl-paired side (**Fig 2B;** t_{15}=2.95, p=0.0099) and preference for the fentanyl over saline side (**Fig 2C;** t_{15}=2.71, p=0.016) compared to vehicle. Intra-NAc raclopride also reduced locomotion (**Fig 2D;** t_{15}=3.04, p=0.0083). In contrast, intra-PFC raclopride had no effect on fentanyl place preference (**Fig 2E-F**) or locomotion (**Fig 2G**).

Both VTA-NAc and VTA-PFC exhibit elevated calcium activity during fentanyl conditioning

Since we found a role for PFC and NAc dopamine receptors in fentanyl CPP, we next investigated upstream VTA signaling directed at each of these target regions. While there is support for dopamine-independent mechanisms of opioid CPP (Hnasko et al. 2005), whether these mechanisms rely on VTA is unknown. Therefore, we targeted VTA-NAc and VTA-PFC projection neurons in a cell type-agnostic manner to investigate their respective roles in fentanyl CPP. We used fiber photometry to measure calcium activity of VTA-NAc and VTA-PFC during fentanyl CPP (**Fig 3A**). First, we established the cell-types captured by our viral approach. We found heterogeneity in projection-specific cell types expressing GCaMP, with 32.5% of VTA-NAc GCaMP-expressing neurons, and 28.4% of VTA-PFC GCaMP-expressing neurons, colocalizing with TH (**Fig 3B**; n=5 mice per projection target group x 3 images per mouse; VTA-NAc vs VTA-PFC t-test, t_8=1.22, p=0.26). We corroborated findings at the protein level with mRNA using the RiboTag mouse. We sequenced ribosome-associated mRNA from projection neurons alongside total VTA, and used enrichment of cell-type marker genes to estimate the proportion of dopamine, glutamate, and GABA neurons. Similar to IHC, ~20% of each projection was enriched for dopamine markers, and the remaining 80% was evenly split between glutamatergic and GABAergic markers (**Supplemental File 1**).

To determine the role for VTA-NAc and VTA-PFC in fentanyl CPP, we first ensured no behavioral differences across the groups. Both VTA-NAc and VTA-PFC GCaMP mice spent a similar amount of time in the fentanyl-paired context during the post-test (**Fig 3C**; VTA-NAc vs VTA-PFC t-test, t_{17}=0.72, p=0.48) and exhibited similar preference for the fentanyl-paired over the saline-paired context (**Fig 3D**; VTA-NAc vs VTA-PFC t-test, t_{17}=0.59, p=0.56). To examine activity of VTA-NAc and VTA-PFC neurons in response to fentanyl

we analyzed photometry data during the conditioning sessions (**Fig 3E**). There were no main effects of conditioning day, so data were averaged across days and analyzed with paired t-test. For both VTA-NAc and VTA-PFC neurons, we found a greater number of calcium transients during fentanyl conditioning relative to saline (VTA-NAc: **Fig 3F**, t_8=4.32, p=0.0025; VTA-PFC: **Fig 3G**, t_4=5.018, p=0.0074). We then analyzed transient frequency during the post-test and found mesolimbic signals resembling reward prediction error. VTA-NAc had reduced transient frequency when the mouse was in the fentanyl-paired context compared to the saline-paired context (**Fig 3H**, t_9=2.32, p=0.046) while VTA-PFC had no significant difference in frequency in the fentanyl- vs saline-paired context (**Fig 3I**, t_8=1.84, p=0.1).

Both VTA-NAc and VTA-PFC exhibit elevated calcium activity during entries to the fentanyl-paired context

Next, we asked if VTA-NAc and VTA-PFC were differentially engaged during entry into the fentanyl-paired context on test days, as others have shown VTA calcium increases during entry to a cocaine-paired context (Calipari et al. 2017). To control for behavioral differences among mice, we only analyzed the first 15 transitions into each side of the chamber for each mouse. Using bootstrapped 95% confidence intervals (Jean-Richard-dit-Bressel et al. 2020), we found increased VTA-NAc activity preceding entries to both the saline- and fentanyl-paired contexts, but the activity was greater in the one second immediately preceding fentanyl-paired entries (**Fig 4A**). In contrast, VTA-PFC neurons exhibited increased activity only preceding fentanyl-paired, but not saline-paired entries (**Fig 4C**). The increased calcium activity in VTA projections during entries to the fentanyl-paired context did not reflect exits from the saline-paired context, since there were no differences in the signal when aligned to region exits (**Fig 4A,C**). We did not identify any signals consistent with extinction, as the increased activity preceding fentanyl-paired region entry was consistent throughout the session for both projections (**Fig 4B,D**). To ensure these effects were consistent across animals, for each animal we calculated the mean zΔF/F over the 1 second immediately preceding region entries (-1 to 0 seconds from entry) and used paired t-tests to compare between saline- and fentanyl-paired entries. During the pre-test, there were no differences in mean zΔF/F preceding region entries for both VTA-NAc (**Fig 4E**) and VTA-PFC (**Fig 4G**), ensuring that the increased activity observed during the post-test is due to context associations and not pre-existing biases. After conditioning, like what we observed with bootstrapped confidence intervals, there was

greater mean zΔF/F in the one second preceding fentanyl-paired entries compared to saline-paired entries for both VTA-NAc (**Fig 4F**, t_9=2.39, p=0.041) and VTA-PFC (**Fig 4H**, t_8=2.53, p=0.035).

Chemogenetic inhibition of VTA-NAc, not VTA-PFC, attenuates fentanyl place preference

Next, we used chemogenetic inhibition to determine whether activity in VTA-NAc and VTA-PFC functionally support fentanyl place preference. We expressed the inhibitory DREADD hM4Gi, or an mCherry control, in either VTA-NAc or VTA-PFC (Timeline in **Fig 5A**). To validate our approach, a subset of mice were injected with DCZ, then with fentanyl to induce cFos expression (**Fig 5B-C**). There was ~50% less cFos in hM4Gi neurons relative to mCherry neurons in both projection populations (**Fig 5D.** hM4Gi vs mCherry: VTA-NAc: 27.47±2.29 vs 15.05±2.03 cFos+ cells; VTA-PFC: 20.17±1.23 vs 9.55±0.93 cFos+ cells; VTA-NAc vs VTA-PFC p=0.42). The remaining mice underwent CPP as before. Using a counterbalanced, within-subject design, mice underwent two post-tests 4 hours apart, each preceded by an injection of either DCZ or vehicle (**Fig 5A**). Chemogenetic inhibition of VTA-NAc reduced time spent in the fentanyl-paired context (**Fig 5E,** vehicle vs DCZ: hM4Gi p=0.036, mCherry p=0.81, Sidak's post hoc) as well as preference for fentanyl- over saline-paired context (**Fig 5F**; vehicle vs DCZ: hM4Gi p=0.018, mCherry p=0.91, Sidak's). This effect was not due to reduced locomotion (**Fig 5G**). In contrast, chemogenetic inhibition of VTA-PFC did not significantly alter fentanyl place preference (**Fig 5H-I**), but did reduce movement counts (**Fig 5J,** vehicle vs DCZ: hM4Gi p=0.037, mCherry p=0.32, Sidak's post hoc,).

DISCUSSION

In this study we investigated mesolimbic and mesocortical regulation of fentanyl-context associations. We showed a role for dopaminergic signaling in both PFC and NAc, where fentanyl place preference is supported by activity at D1 receptors in PFC, and activity at D2 receptors in NAc. To investigate potential roles for other neurotransmitters in addition to dopamine, we targeted VTA-NAc and VTA-PFC neurons in a cell type-agnostic manner. Despite increased calcium activity in both mesolimbic and mesocortical neurons during fentanyl CPP, only chemogenetic inhibition of mesolimbic, not mesocortical neurons, attenuated fentanyl place preference. Together these data demonstrate that fentanyl-context associations engage both dopamine and non-dopamine neurons, but only VTA-NAc neurons directly modulate the behavior.

Divergent dopaminergic signaling mechanisms in NAc and PFC during fentanyl CPP

To address gaps in knowledge regarding dopaminergic signaling mechanisms that promote fentanyl CPP, we administered local dopamine receptor antagonists during the post-test. This approach allowed us to understand receptor mechanisms in the expression of place preference without also influencing learning of drug-context associations. In PFC, we found an effect of D1 but not D2 receptor antagonism. This is somewhat unsurprising, as D1R is more abundant than D2R in PFC (Santana et al. 2009), though there is some overlap between these populations, with ~14% of D1R+ PFC neurons co-expressing D2R (Wei et al. 2018). Our findings with fentanyl also resemble those with cocaine, as blocking D1R but not D2R in PFC reduces the expression of cocaine CPP (Shinohara et al. 2017). While the present study is the first to investigate this in fentanyl CPP, others have shown PFC D1R blockade attenuates cue-induced heroin seeking after self-administration (See 2009). Taken together, these findings suggest that dopaminergic mechanisms of drug-cue recognition in PFC may be consistent across drug classes and behavioral paradigms.

In NAc, we found that blocking D2R, but not D1R, inhibited the expression of fentanyl CPP. Both D1 and D2 receptors are equally abundant on GABAergic medium spiny neurons (MSNs) in NAc with little to no overlap in their expression patterns (Reiner et al. 2024). While D1-MSNs are classically known for promoting motivation and reward seeking, there is evidence to suggest these processes can also be mediated by D2-MSNs (Soares-Cunha et al. 2016; Gallo et al. 2018). Furthermore D2R, unlike D1R, is expressed on other cell types in the striatum besides MSNs, such as dopaminergic afferents (Sesack et al. 1998; Benoit-Marand et al. 2001) and cholinergic interneurons (Yan et al. 1997; Maurice et al. 2004). As such, D2R inhibition likely has a more widespread effect on intra-NAc signaling as compared to D1R inhibition, which could further explain the behavioral differences resulting from these antagonists. An additional effect of intra-NAc dopamine receptor blockade is that both antagonists reduced locomotion during the post-test. This effect has been previously reported, with intra-NAc SCH23390 or raclopride reducing locomotion in a CPP apparatus (Young et al. 2014). Importantly, we believe the observed reduction in fentanyl preference following intra-NAc D2R blockade is likely not driven by reduced locomotion, as intra-NAc D1R blockade reduced locomotion without affecting fentanyl preference.

Mesolimbic, not mesocortical, signaling functionally supports fentanyl place preference

Having determined a role for dopaminergic signaling in both NAc and PFC during fentanyl CPP, we next investigated activity of upstream VTA neurons that project to each of these regions. Prior research

suggests that opioid CPP is not wholly dependent on dopaminergic mechanisms. Dopamine deficient mice (Hnasko et al. 2005) and D1R-knockout mice (Ting-A-Kee et al. 2013) can both acquire morphine CPP, but the extent to which these effects are mediated by the VTA is unknown. As such, we broadened our investigation to include other neuron types in mesolimbic and mesocortical pathways besides just dopamine neurons. To achieve this, we opted for a projection-specific, but cell type-agnostic AAV approach that enriches for non-dopamine neurons, as midbrain dopamine neurons are not efficiently captured by most AAV serotypes (Tervo et al. 2016). Indeed, our immunolabelling revealed ~30% of GCaMP-expressing neurons were TH-positive in both projections. This effect was further corroborated by our Ribotag RNAseq, showing about 20% of each projection expressed dopamine markers, and the remaining 80% glutamate and GABA markers. At both RNA and protein level, our AAV strategy captured a lower proportion of dopamine neurons as compared to other approaches. For example, retrograde tracer Fluorogold reveals ~70% of mouse VTA projection neurons are TH+ (Taylor et al. 2014), while Cre-expressing canine adenoviruses show ~60% VTA-NAc are TH+ vs 40% VTA-PFC (Beier et al. 2015). We suspect our low proportion of TH-expression in VTA projection neurons reflects AAV transduction inefficiency and is not a true reflection of the endogenous proportion of dopamine neurons in these projections. However, by enriching for multiple cell types in these pathways, we reveal ways in which diverse VTA cell types can support fentanyl CPP through their projections to other brain regions.

In the present study we found both VTA-NAc and VTA-PFC had increased calcium activity during fentanyl exposure, consistent with classic opioid-mediated disinhibition in the VTA. We also found VTA-NAc exhibited decreased transient frequency when mice are in their fentanyl-paired context, reminiscent of a reward prediction error signal. Because others have shown increased calcium activity in VTA neurons and their downstream projections to NAc during entries to a cocaine-paired context (Calipari et al. 2017), we aligned our calcium signal to region transitions to look at projection-specific VTA activity during entries to the fentanyl-paired context. We found similar effects in both VTA-NAc and VTA-PFC neurons, where both had greater calcium activity immediately preceding fentanyl-paired entries compared to saline-paired entries. To determine whether this activity promotes fentanyl CPP or is a consequence of CPP, we chemogenetically inhibited either projection during the post-test. Surprisingly, we found only chemogenetic inhibition of VTA-NAc, but not VTA-PFC neurons attenuated fentanyl place preference. Collectively, this suggests that while mesocortical neurons are engaged by the behavior, their causal role is more limited relative to mesolimbic neurons.

Beyond dopamine, VTA glutamate and GABA projection neurons have known roles in motivated behavior and reinforcement learning (Root et al. 2014, 2020; Wang et al. 2015; Yoo et al. 2016; Zell et al. 2020; Warlow et al. 2024). VTA glutamate neurons can modulate oxycodone seeking through their local connections to mesolimbic dopamine neurons (McGovern et al. 2023), and both VTA glutamate and GABA neurons undergo diverse transcriptional adaptations after fentanyl self-administration (Fox et al. 2024). Downstream, blocking GABA and glutamate receptors in NAc can attenuate CPP (Popik and Kolasiewicz 1999; Maguire et al. 2014; Qi et al. 2015), however these effects cannot be ascribed to VTA neurotransmission. Here, our data that overrepresent non-dopamine neurons indicate some of these glutamatergic and GABAergic effects may be driven by the VTA. While VTA-NAc glutamate opposes cocaine seeking (Barbano et al. 2024) this may not extend to fentanyl. Additional studies should investigate the role for neurotransmitter-defined cell types across a variety of opioid administration paradigms, as our data indicate mesolimbic neurons as a whole are important for the expression of fentanyl-context associations.

Conclusions

Here we demonstrate that projection-specific VTA neurons drive fentanyl-context associations through diverse signaling, providing a unique viewpoint of VTA representations of opioid behaviors. These experiments lay the foundation for further investigation into cell type-specific encoding of opioid-context associations in the VTA. These findings provide necessary insight to the circuit-level neuroadaptations that promote fentanyl-context associations, thus improving our understanding of potential neural mechanisms underlying OUD.

Acknowledgements

The authors thank the Penn State College of Medicine Genome Sciences Core (RRID:SCR_021123) and Advanced Light Microscopy Core (RRID:SCR_022526).

Author Contributions

AM and MEF designed the experiments. AM and FAA performed surgeries. AM, HS, LBM, LDF, and SP performed behavior experiments. MEF performed RNA isolation. AM and KD counted cells. AM and MEF performed data analysis. AM and MEF wrote the manuscript and prepared the figures with input from all authors.

Funding

This work was supported by NIH grant DA058661 awarded to MEF.

Competing Interests The authors have nothing to disclose.

Data and code availability

Code is available at gitihub.com/mfoxlab. RNAseq data have been deposited at GEO and are publicly available as of the date of publication. Other data are available upon reasonable request addressed to the corresponding author.

Figures and Legends

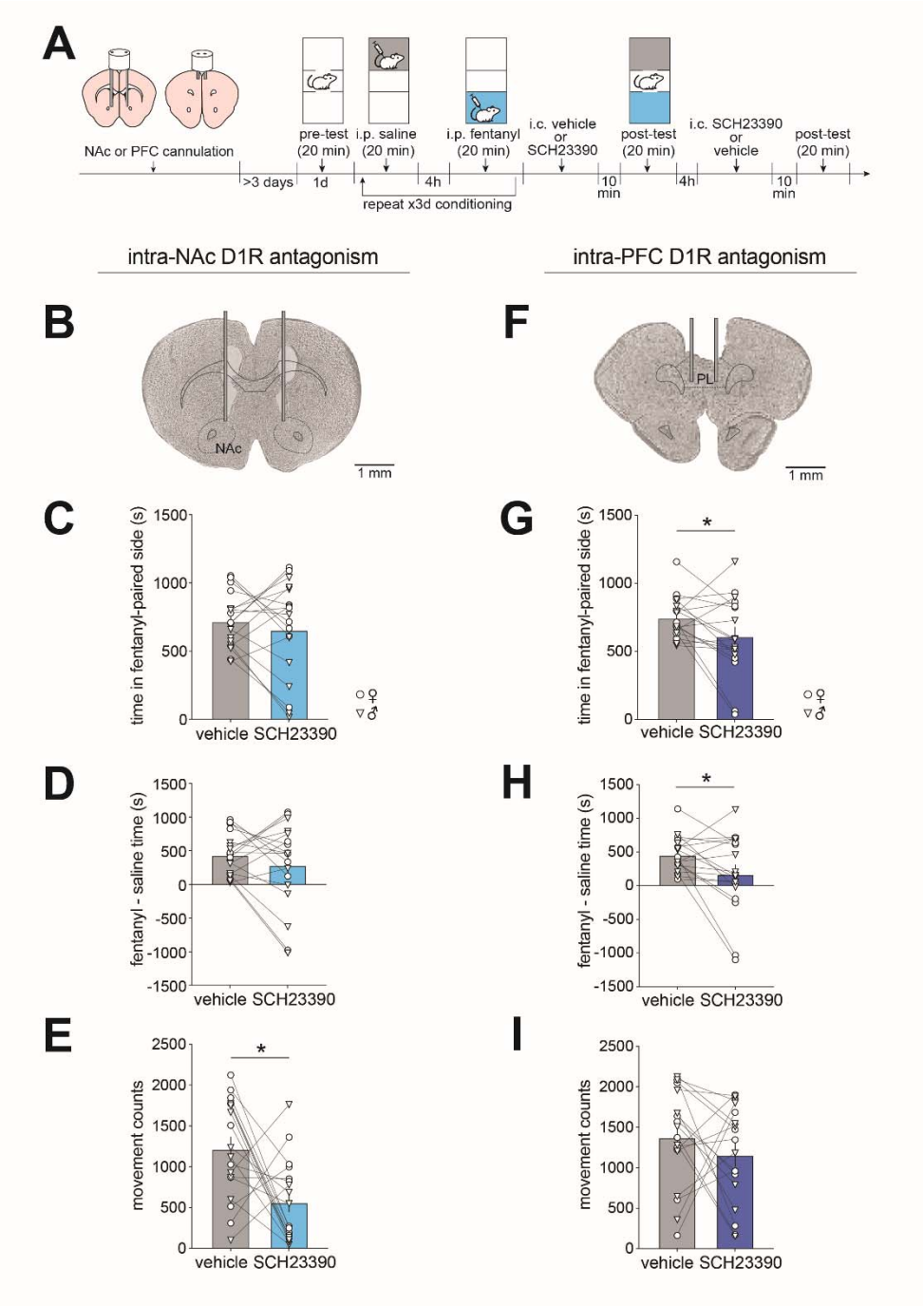

Figure 1. D1R antagonism in PFC, not NAc, attenuates fentanyl place preference. (A) Timeline for intracranial SCH23390 experiments. Mice received a bilateral infusion cannula in either NAc or PFC, and underwent fentanyl CPP at least 3 days later. Ten minutes prior to each post-test, mice received intracranial SCH23390 (0.2 ug / 0.5 uL infused over 1 minute) or vehicle in a counterbalanced repeated-measures design. (**B**) Representative image of NAc cannula placement. Intra-NAc SCH23390 had no effect on (**C**) time in the fentanyl-paired context, or (**D**) preference for the fentanyl- over saline-paired context. (**E**) Intra-NAc SCH23390 reduced movement counts relative to vehicle (n=18, *, p=0.01). (**F**) Representative image of PFC cannula placement (PL, prelimbic cortex). Intra-PFC SCH23390 reduced (**G**) time in the fentanyl-paired context (n=18, *, p=0.045) and (**H**) preference for the fentanyl- over saline-paired context (*, p=0.031) relative to vehicle. (**I**) Intra-PFC SCH23390 had no effect on movement counts. Data are presented as mean±SEM with individual mice overlaid. Circles represent data points from females, and triangles from males.

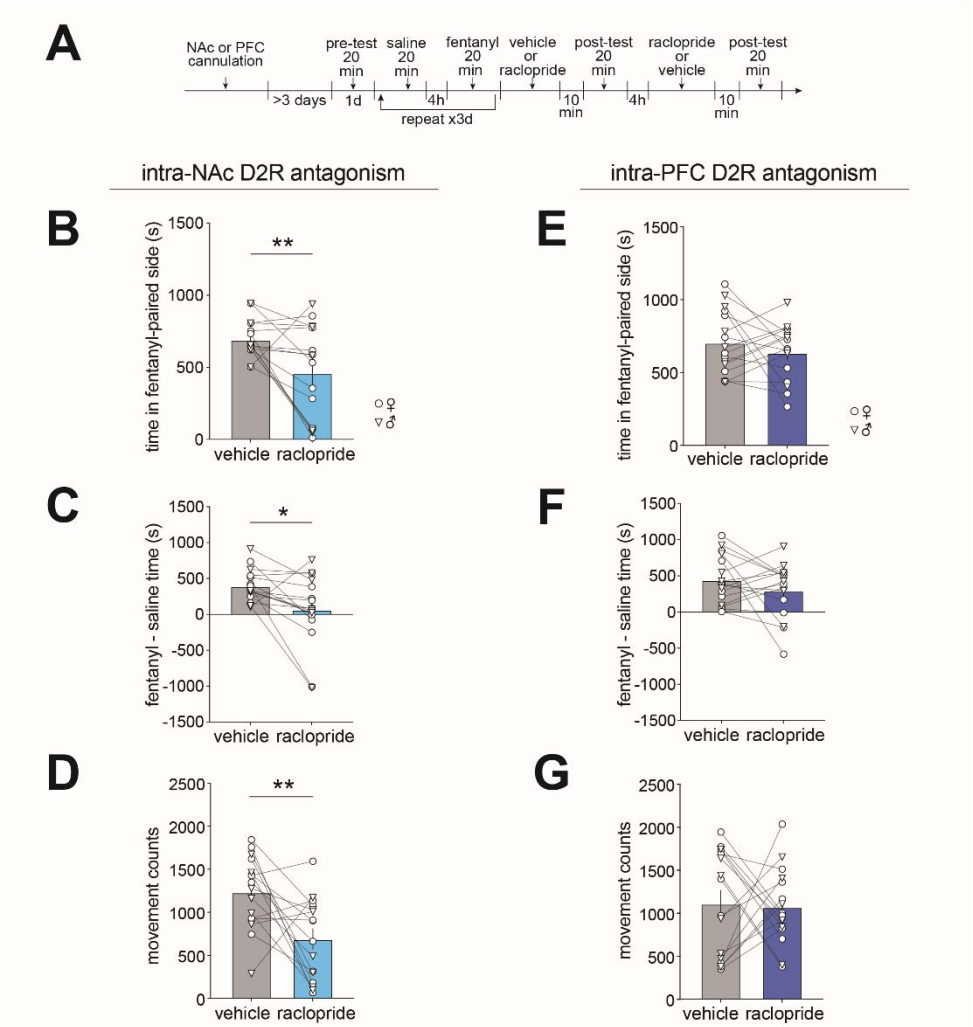

Figure 2. D2R antagonism in NAc, not PFC, attenuates fentanyl place preference. (**A**) Timeline for intracranial raclopride experiments (1 ug raclopride / 0.5 uL infused over 1 minute). Intra-NAc raclopride reduced (**B**) time in the fentanyl-paired context (n=16, **, p=0.0099), (**C**) preference for the fentanyl- over saline-paired context (*, p=0.0116) and (**D**) movement counts (**, p=0.0083) relative to vehicle. Intra-PFC raclopride had no effect on (**E**) time in the fentanyl-paired context, (**F**) preference for the fentanyl- over saline-paired context, or (**G**) movement counts, relative to vehicle (n=16). Data are presented as mean±SEM with individual mice overlaid. Circles represent data points from females, and triangles from males.

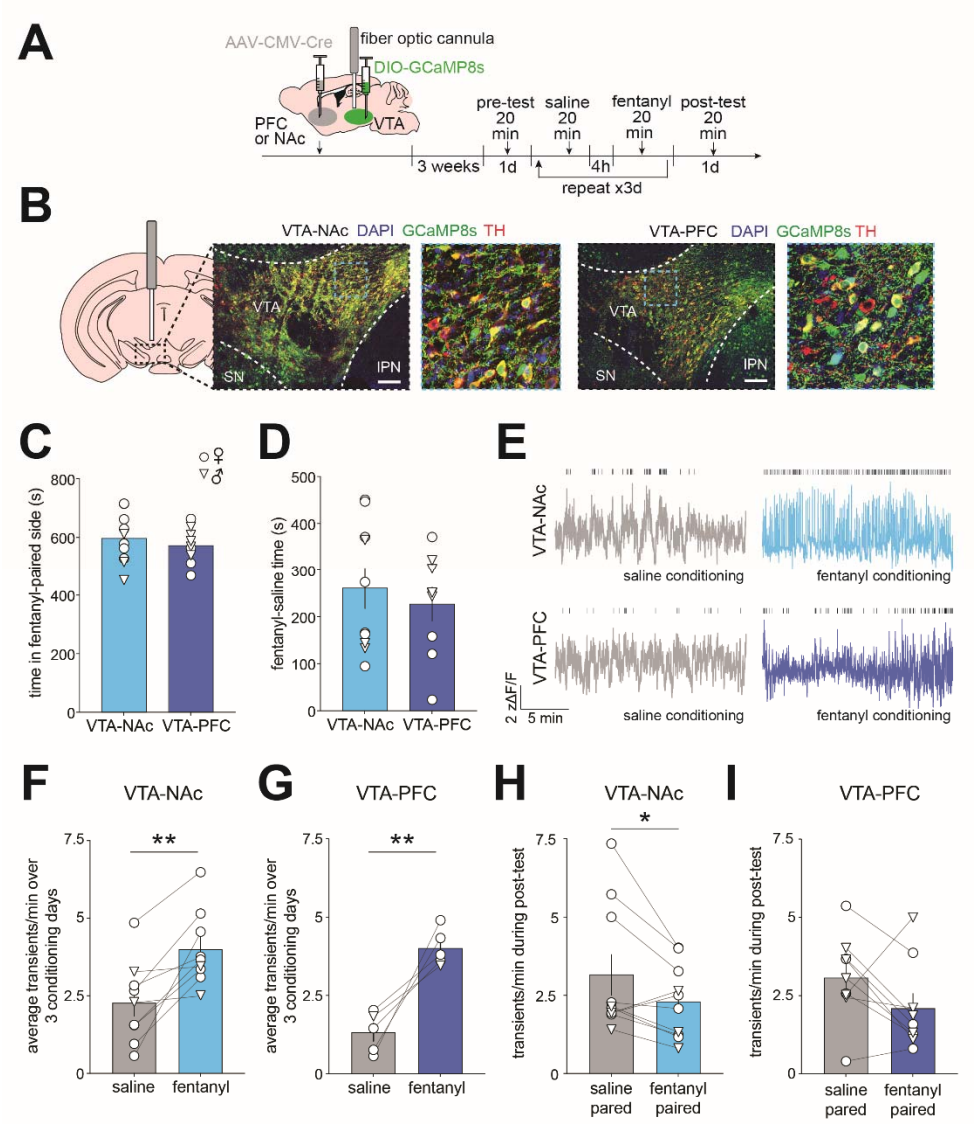

Figure 3. VTA-NAc and VTA-PFC have elevated calcium activity in response to fentanyl exposure. (**A**) Timeline for projection-specific VTA GCaMP fiber photometry experiments. Mice received retrograde Cre in either the PFC or NAc, and Cre-dependent GCaMP8s in VTA, with a fiber optic cannula implanted directly above VTA. Three weeks later, mice underwent fentanyl CPP and VTA GCaMP signal was recorded during all sessions. (**B**) Representative images depicting GCaMP expression in VTA-NAc and VTA-PFC with immunostaining for TH (SN, substantia nigra, IPN, interpeduncular nucleus). (**C**) VTA-NAc and VTA-PFC GCaMP groups did not differ in time spent in fentanyl-paired side during the post-test, or (**D**) preference for the fentanyl- over saline-paired context (VTA-NAc n=10, VTA-PFC n=9). (**E**) Representative calcium traces from VTA-NAc (top) and VTA-PFC (bottom) during saline conditioning (left) and fentanyl conditioning (right). Ticks above the trace indicate identified calcium transients. (**F**) In VTA-NAc, fentanyl increases transient frequency (n=9, average over 3 conditioning days, **, p=0.0025) (**G**) In VTA-PFC, fentanyl increases transient frequency (n=5, average over 3 conditioning days, **, p=0.0074). (**H**) During the post-test, VTA-NAc has reduced transient frequency when the mouse is in the fentanyl- compared to saline-paired context (n=10; *, p=0.046) (**I**) No difference in VTA-PFC transient frequency in saline-paired vs fentanyl-paired context (n=9; p=0.1). Data are presented as mean±SEM with individual mice overlaid. Circles represent data points from females, and triangles from males.

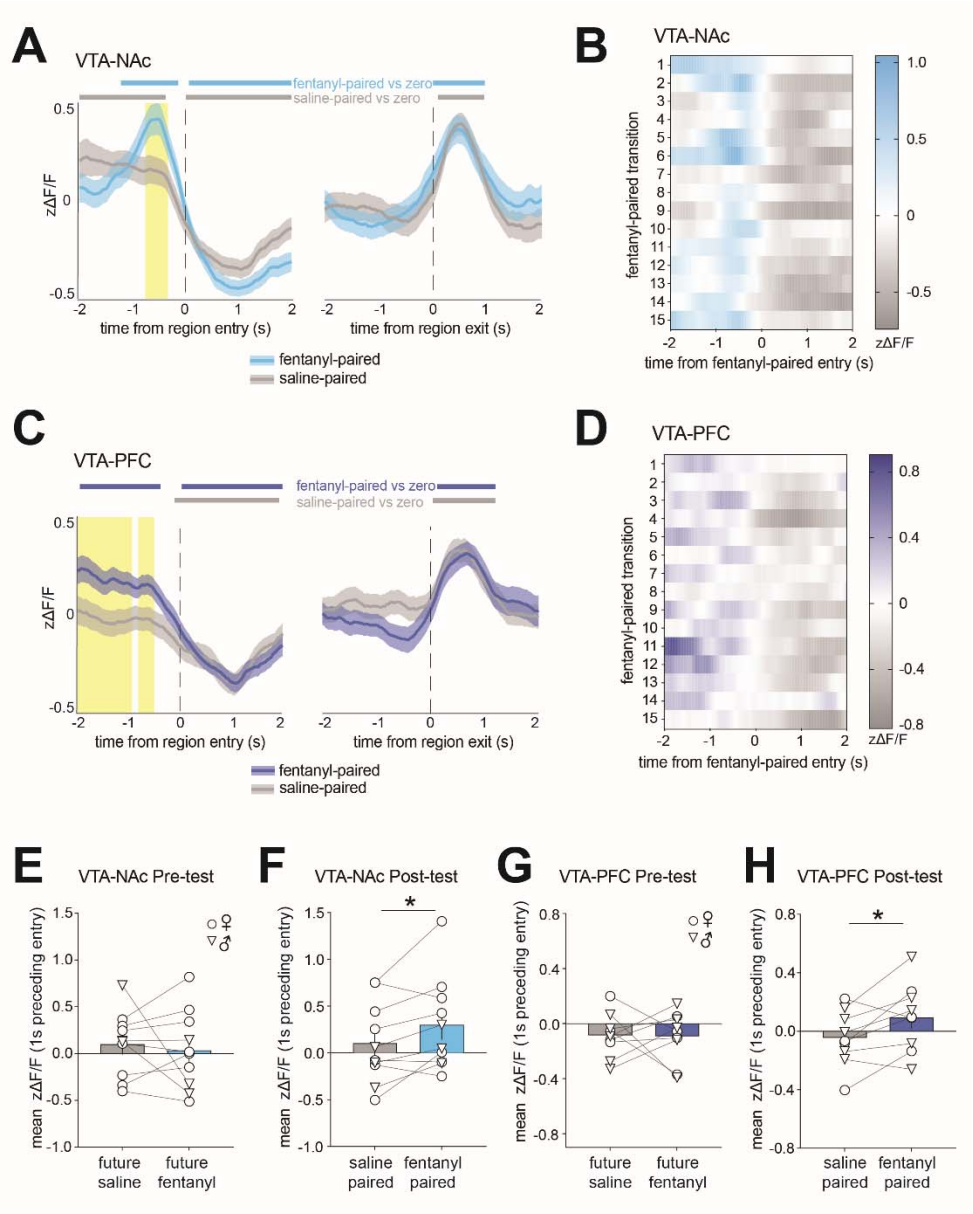

Figure 4. VTA-NAc and VTA-PFC have elevated calcium activity during entries to the fentanyl-paired context. (**A**) Average zΔF/F for all VTA-NAc mice for 4 seconds surrounding the first 15 entries (left) or exits (right) to the saline-paired (gray trace) or fentanyl-paired (blue trace) context. Vertical dotted line represents the time of entry/exit. Using bootstrapped 95% confidence intervals, gray and blue horizontal bars represent where the gray and blue traces (saline-paired and fentanyl-paired, respectively) significantly differ from 0, and yellow shaded area represents where the two traces significantly differ from one another. (**B**) Heatmap of VTA-NAc activity for the 4 seconds surrounding the first 15 entries into the fentanyl-paired region. Color represents zΔF/F averaged across all VTA-NAc mice. (**C-D**) Same as A-B, but for VTA-PFC. (**E**) During the pre-test for VTA-NAc there is no difference in mean zΔF/F over the 1 second preceding entry to either context. (**F**) During the post-test for VTA-NAc there is greater calcium activity in the 1 second preceding entries to fentanyl-paired vs saline-paired context (n=10; *, p=0.04). (**G-H**) Same as E-F, but for VTA-PFC (n=9, *, p=0.035). Data are presented as mean±SEM with individual mice overlaid. Circles represent data points from females, and triangles from males.

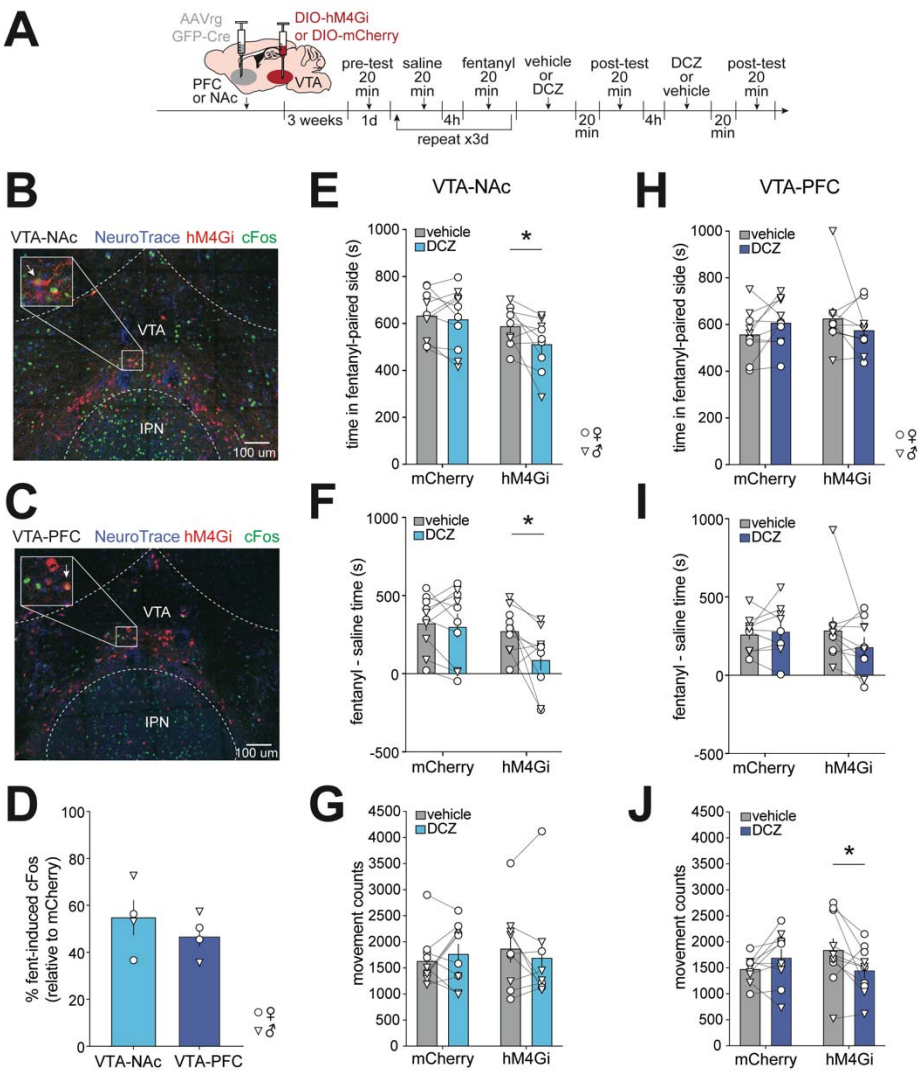

Figure 5. Chemogenetic inhibition of VTA-NAc, not VTA-PFC, attenuates fentanyl place preference. (**A**) Timeline for chemogenetic experiments. Mice received retrograde-Cre in either PFC or NAc, and Cre-dependent hM4Gi, or Cre-dependent mCherry, in VTA. Twenty minutes prior to each post-test, mice received DCZ (0.1 mg/kg i.p.) or vehicle in a counterbalanced repeated-measures design. Representative images of hM4Gi and cFos expression in (**B**) VTA-NAc and (**C**) VTA-PFC. (**D**) Both VTA-NAc and VTA-PFC exhibit similar reduction in fentanyl-induced cFos expression in hM4Gi relative to mCherry neurons (n=3-4 mice/virus/projection). (**E**) Time in fentanyl-paired context (*, p=0.036), (**F**) preference for fentanyl- over saline-paired context (*, p=0.018), and (**G**) total movement counts after treatment with vehicle (gray) and DCZ (light blue) in mice expressing mCherry (n=10) or hM4Gi (n=9) in VTA-NAc. (**H**) Time in fentanyl-paired context, (**I**) preference for fentanyl- over saline-paired context, and (**J**) total movement counts (*, p=0.037) after treatment with vehicle (gray) and DCZ (dark blue) in mice expressing mCherry (n=10) or hM4Gi (n=10) in VTA-PFC. Data are presented as mean±SEM with individual mice overlaid. Circles represent data points from females, and triangles from males.

References

Barbano MF, Qi J, Chen E, et al (2024) VTA glutamatergic projections to the nucleus accumbens suppress psychostimulant-seeking behavior. Neuropsychopharmacol 49:1905–1915. https://doi.org/10.1038/s41386-024-01905-3

Beier KT, Steinberg EE, DeLoach KE, et al (2015) Circuit Architecture of VTA Dopamine Neurons Revealed by Systematic Input-Output Mapping. Cell 162:622–634. https://doi.org/10.1016/j.cell.2015.07.015

Benoit-Marand M, Borrelli E, Gonon F (2001) Inhibition of Dopamine Release Via Presynaptic D2 Receptors: Time Course and Functional Characteristics *In Vivo*. J Neurosci 21:9134–9141. https://doi.org/10.1523/JNEUROSCI.21-23-09134.2001

Bossert JM, Liu SY, Lu L, Shaham Y (2004) A Role of Ventral Tegmental Area Glutamate in Contextual Cue-Induced Relapse to Heroin Seeking. J Neurosci 24:10726–10730. https://doi.org/10.1523/JNEUROSCI.3207-04.2004

Calipari ES, Juarez B, Morel C, et al (2017) Dopaminergic dynamics underlying sex-specific cocaine reward. Nat Commun 8:13877. https://doi.org/10.1038/ncomms13877

Chaudhury D, Walsh JJ, Friedman AK, et al (2013) Rapid regulation of depression-related behaviours by control of midbrain dopamine neurons. Nature 493:532–536. https://doi.org/10.1038/nature11713

Czachowski CL, Chappell AM, Samson HH (2001) Effects of Raclopride in the Nucleus Accumbens on Ethanol Seeking and Consumption. Alcoholism Clin & Exp Res 25:1431–1440. https://doi.org/10.1111/j.1530-0277.2001.tb02144.x

Dobin A, Davis CA, Schlesinger F, et al (2013) STAR: ultrafast universal RNA-seq aligner. Bioinformatics 29:15–21. https://doi.org/10.1093/bioinformatics/bts635

Doyle MA, Mazei-Robison MS (2021) Opioid-Induced Molecular and Cellular Plasticity of Ventral Tegmental Area Dopamine Neurons. Cold Spring Harb Perspect Med 11:a039362. https://doi.org/10.1101/cshperspect.a039362

Eshleman AJ, Nagarajan S, Wolfrum KM, et al (2020) Affinity, potency, efficacy, selectivity, and molecular modeling of substituted fentanyls at opioid receptors. Biochemical Pharmacology 182:114293. https://doi.org/10.1016/j.bcp.2020.114293

Finlay JM, Jakubovic A, Phillips AG, Fibiger HC (1988) Fentanyl-induced conditional place preference: lack of associated conditional neurochemical events. Psychopharmacology 96:534–540. https://doi.org/10.1007/BF02180036

Fitzgerald ND, Day JJ (2025) Neuronal heterogeneity in the ventral tegmental area: Distinct contributions to reward circuitry and motivated behavior. Addiction Neuroscience 14:100191. https://doi.org/10.1016/j.addicn.2024.100191

Fox ME, Chandra R, Menken MS, et al (2020) Dendritic remodeling of D1 neurons by RhoA/Rho-kinase mediates depression-like behavior. Mol Psychiatry 25:1022–1034. https://doi.org/10.1038/s41380-018-0211-5

Fox ME, Montemarano A, Ostman AE, et al (2024) Transcriptional signatures of fentanyl use in the mouse ventral tegmental area. Addiction Biology 29:e13403. https://doi.org/10.1111/adb.13403

Fox ME, Wulff AB, Franco D, et al (2023) Adaptations in Nucleus Accumbens Neuron Subtypes Mediate Negative Affective Behaviors in Fentanyl Abstinence. Biological Psychiatry 93:489–501. https://doi.org/10.1016/j.biopsych.2022.08.023

Friedman AK, Walsh JJ, Juarez B, et al (2014) Enhancing Depression Mechanisms in Midbrain Dopamine Neurons Achieves Homeostatic Resilience. Science 344:313–319. https://doi.org/10.1126/science.1249240

Gallo EF, Meszaros J, Sherman JD, et al (2018) Accumbens dopamine D2 receptors increase motivation by decreasing inhibitory transmission to the ventral pallidum. Nat Commun 9:1086. https://doi.org/10.1038/s41467-018-03272-2

Hiroi N, White NM (1991) The amphetamine conditioned place preference: differential involvement of dopamine receptor subtypes and two dopaminergic terminal areas. Brain Research 552:141–152. https://doi.org/10.1016/0006-8993(91)90672-I

Hnasko TS, Sotak BN, Palmiter RD (2005) Morphine reward in dopamine-deficient mice. Nature 438:854–857. https://doi.org/10.1038/nature04172

Huuki-Myers LA, Montgomery KD, Kwon SH, et al (2025) Benchmark of cellular deconvolution methods using a multi-assay dataset from postmortem human prefrontal cortex. Genome Biol 26:88. https://doi.org/10.1186/s13059-025-03552-3

Jean-Richard-dit-Bressel P, Clifford CWG, McNally GP (2020) Analyzing Event-Related Transients: Confidence Intervals, Permutation Tests, and Consecutive Thresholds. Front Mol Neurosci 13:14. https://doi.org/10.3389/fnmol.2020.00014

Juarez B, Han M-H (2016) Diversity of Dopaminergic Neural Circuits in Response to Drug Exposure. Neuropsychopharmacol 41:2424–2446. https://doi.org/10.1038/npp.2016.32

Kawahara Y, Ohnishi YN, Ohnishi YH, et al (2021) Distinct Role of Dopamine in the PFC and NAc During Exposure to Cocaine-Associated Cues. International Journal of Neuropsychopharmacology 24:988–1001. https://doi.org/10.1093/ijnp/pyab067

Kawasaki SS, Liebschutz JM, Murray-Krezan C, et al (2026) Barriers to Buprenorphine Initiation in Patients Using Fentanyl. JAMA Netw Open 9:e2552136. https://doi.org/10.1001/jamanetworkopen.2025.52136

Kelly E, Sutcliffe K, Cavallo D, et al (2023) The anomalous pharmacology of fentanyl. British J Pharmacology 180:797–812. https://doi.org/10.1111/bph.15573

Koob GF, Volkow ND (2010) Neurocircuitry of Addiction. Neuropsychopharmacol 35:217–238. https://doi.org/10.1038/npp.2009.110

Lammel S, Hetzel A, Häckel O, et al (2008) Unique Properties of Mesoprefrontal Neurons within a Dual Mesocorticolimbic Dopamine System. Neuron 57:760–773. https://doi.org/10.1016/j.neuron.2008.01.022

Lerner TN, Shilyansky C, Davidson TJ, et al (2015) Intact-Brain Analyses Reveal Distinct Information Carried by SNc Dopamine Subcircuits. Cell 162:635–647. https://doi.org/10.1016/j.cell.2015.07.014

Lewis DA, Melchitzky DS, Sesack SR, et al (2001) Dopamine transporter immunoreactivity in monkey cerebral cortex: Regional, laminar, and ultrastructural localization. J of Comparative Neurology 432:119–136. https://doi.org/10.1002/cne.1092

Liao Y, Smyth GK, Shi W (2014) featureCounts: an efficient general purpose program for assigning sequence reads to genomic features. Bioinformatics 30:923–930. https://doi.org/10.1093/bioinformatics/btt656

Maguire EP, Macpherson T, Swinny JD, et al (2014) Tonic Inhibition of Accumbal Spiny Neurons by Extrasynaptic α4βδ $GABA_A$ Receptors Modulates the Actions of Psychostimulants. J Neurosci 34:823–838. https://doi.org/10.1523/JNEUROSCI.3232-13.2014

Margolis EB, Lock H, Chefer VI, et al (2006) κ opioids selectively control dopaminergic neurons projecting to the prefrontal cortex. Proc Natl Acad Sci USA 103:2938–2942. https://doi.org/10.1073/pnas.0511159103

Maurice N, Mercer J, Chan CS, et al (2004) D_2 Dopamine Receptor-Mediated Modulation of Voltage-Dependent Na^+ Channels Reduces Autonomous Activity in Striatal Cholinergic Interneurons. J Neurosci 24:10289–10301. https://doi.org/10.1523/JNEUROSCI.2155-04.2004

McGovern DJ, Polter AM, Prévost ED, et al (2023) Ventral tegmental area glutamate neurons establish a mu-opioid receptor gated circuit to mesolimbic dopamine neurons and regulate opioid-seeking behavior. Neuropsychopharmacol 48:1889–1900. https://doi.org/10.1038/s41386-023-01637-w

McGovern DJ, Polter AM, Root DH (2021) Neurochemical Signaling of Reward and Aversion to Ventral Tegmental Area Glutamate Neurons. J Neurosci 41:5471–5486. https://doi.org/10.1523/JNEUROSCI.1419-20.2021

Montemarano A, Fox LD, Alkhaleel FA, et al (2025) A Drd1-cre mouse line with nucleus accumbens gene dysregulation exhibits blunted fentanyl seeking. Neuropsychopharmacology 50:1993–2005. https://doi.org/10.1101/2025.02.14.638324

Morison SL, Doster LB, Vigotsky AD, et al (2025) Recruitment of specific dopamine neuron sub-circuits by opioids. Addiction Neuroscience 17:100233. https://doi.org/10.1016/j.addicn.2025.100233

O'Neal TJ, Bernstein MX, MacDougall DJ, Ferguson SM (2022) A Conditioned Place Preference for Heroin Is Signaled by Increased Dopamine and Direct Pathway Activity and Decreased Indirect Pathway Activity in the Nucleus Accumbens. J Neurosci 42:2011–2024. https://doi.org/10.1523/JNEUROSCI.1451-21.2021

Oriol L, Chao M, Kollman GJ, et al (2025) Ventral tegmental area interneurons revisited: GABA and glutamate projection neurons make local synapses. eLife 13:RP100085. https://doi.org/10.7554/eLife.100085

Phillips RA, Tuscher JJ, Black SL, et al (2022) An atlas of transcriptionally defined cell populations in the rat ventral tegmental area. Cell Reports 39:110616. https://doi.org/10.1016/j.celrep.2022.110616

Popik P, Kolasiewicz W (1999) Mesolimbic NMDA receptors are implicated in the expression of conditioned morphine reward: Naunyn-Schmiedeberg's Arch Pharmacol 359:288–294. https://doi.org/10.1007/PL00005354

Qi C, Wang X, Ge F, et al (2015) mGLuR 5 in the nucleus accumbens shell regulates morphine-associated contextual memory through reactive oxygen species signaling. Addiction Biology 20:927–940. https://doi.org/10.1111/adb.12222

Reiner BC, Chehimi SN, Merkel R, et al (2024) A single-nucleus transcriptomic atlas of medium spiny neurons in the rat nucleus accumbens. Sci Rep 14:18258. https://doi.org/10.1038/s41598-024-69255-0

Ritchie ME, Phipson B, Wu D, et al (2015) limma powers differential expression analyses for RNA-sequencing and microarray studies. Nucleic Acids Research 43:e47–e47. https://doi.org/10.1093/nar/gkv007

Root DH, Barker DJ, Estrin DJ, et al (2020) Distinct Signaling by Ventral Tegmental Area Glutamate, GABA, and Combinatorial Glutamate-GABA Neurons in Motivated Behavior. Cell Reports 32:108094. https://doi.org/10.1016/j.celrep.2020.108094

Root DH, Mejias-Aponte CA, Qi J, Morales M (2014) Role of Glutamatergic Projections from Ventral Tegmental Area to Lateral Habenula in Aversive Conditioning. J Neurosci 34:13906–13910. https://doi.org/10.1523/JNEUROSCI.2029-14.2014

Santana N, Mengod G, Artigas F (2009) Quantitative Analysis of the Expression of Dopamine D1 and D2 Receptors in Pyramidal and GABAergic Neurons of the Rat Prefrontal Cortex. Cerebral Cortex 19:849–860. https://doi.org/10.1093/cercor/bhn134

See RE (2009) Dopamine D1 receptor antagonism in the prelimbic cortex blocks the reinstatement of heroin-seeking in an animal model of relapse. Int J Neuropsychopharm 12:431. https://doi.org/10.1017/S1461145709000054

Sesack SR, Hawrylak VA, Matus C, et al (1998) Dopamine Axon Varicosities in the Prelimbic Division of the Rat Prefrontal Cortex Exhibit Sparse Immunoreactivity for the Dopamine Transporter. J Neurosci 18:2697–2708. https://doi.org/10.1523/JNEUROSCI.18-07-02697.1998

Sherathiya VN, Schaid MD, Seiler JL, et al (2021) GuPPy, a Python toolbox for the analysis of fiber photometry data. Sci Rep 11:24212. https://doi.org/10.1038/s41598-021-03626-9

Shinohara F, Kamii H, Minami M, Kaneda K (2017) The Role of Dopaminergic Signaling in the Medial Prefrontal Cortex for the Expression of Cocaine-Induced Conditioned Place Preference in Rats. Biological & Pharmaceutical Bulletin 40:1983–1989. https://doi.org/10.1248/bpb.b17-00614

Shippenberg TS, Bals-Kubik R, Herz A (1993) Examination of the neurochemical substrates mediating the motivational effects of opioids: Role of the mesolimbic dopamine system and D-1 vs. D-2 dopamine receptors. The Journal of Pharmacology and Experimental Therapeutics 265:53–59. https://doi.org/10.1016/S0022-3565(25)38109-7

Simmons SC, Wheeler K, Mazei-Robison MS (2019) Determination of circuit-specific morphological adaptations in ventral tegmental area dopamine neurons by chronic morphine. Mol Brain 12:10. https://doi.org/10.1186/s13041-019-0435-6

Smith T, Heger A, Sudbery I (2017) UMI-tools: modeling sequencing errors in Unique Molecular Identifiers to improve quantification accuracy. Genome Res 27:491–499. https://doi.org/10.1101/gr.209601.116

Soares-Cunha C, Coimbra B, David-Pereira A, et al (2016) Activation of D2 dopamine receptor-expressing neurons in the nucleus accumbens increases motivation. Nat Commun 7:11829. https://doi.org/10.1038/ncomms11829

Socias ME, Wood E, Le Foll B, et al (2022) Impact of fentanyl use on initiation and discontinuation of methadone and buprenorphine/naloxone among people with prescription-type opioid use disorder: secondary analysis of a Canadian treatment trial. Addiction 117:2662–2672. https://doi.org/10.1111/add.15954

Spencer MR, Garnett MF, Miniño AM (2024) Drug Overdose Deaths in the United States, 2002–2022. NCHS Data Brief, no 491 Hyattsville, MD: National Center for Health Statistics.: https://doi.org/10.15620/cdc:135849

Spina L, Fenu S, Longoni R, et al (2006) Nicotine-conditioned single-trial place preference: selective role of nucleus accumbens shell dopamine D1 receptors in acquisition. Psychopharmacology 184:447–455. https://doi.org/10.1007/s00213-005-0211-4

Sutcliffe KJ, Corey RA, Alhosan N, et al (2022) Interaction With the Lipid Membrane Influences Fentanyl Pharmacology. Adv Drug Alcohol Res 2:10280. https://doi.org/10.3389/adar.2022.10280

Tan KR, Yvon C, Turiault M, et al (2012) GABA Neurons of the VTA Drive Conditioned Place Aversion. Neuron 73:1173–1183. https://doi.org/10.1016/j.neuron.2012.02.015

Taylor SR, Badurek S, Dileone RJ, et al (2014) GABAergic and glutamatergic efferents of the mouse ventral tegmental area. J of Comparative Neurology 522:3308–3334. https://doi.org/10.1002/cne.23603

Tervo DGR, Hwang B-Y, Viswanathan S, et al (2016) A Designer AAV Variant Permits Efficient Retrograde Access to Projection Neurons. Neuron 92:372–382. https://doi.org/10.1016/j.neuron.2016.09.021

Ting-A-Kee R, Mercuriano LE, Vargas-Perez H, et al (2013) Dopamine D1 receptors are not critical for opiate reward but can mediate opiate memory retrieval in a state-dependent manner. Behavioural Brain Research 247:174–177. https://doi.org/10.1016/j.bbr.2013.03.026

Vafaie N, Kober H (2022) Association of Drug Cues and Craving With Drug Use and Relapse: A Systematic Review and Meta-analysis. JAMA Psychiatry 79:641. https://doi.org/10.1001/jamapsychiatry.2022.1240

van Zessen R, Phillips JL, Budygin EA, Stuber GD (2012) Activation of VTA GABA Neurons Disrupts Reward Consumption. Neuron 73:1184–1194. https://doi.org/10.1016/j.neuron.2012.02.016

Wang H-L, Qi J, Zhang S, et al (2015) Rewarding Effects of Optical Stimulation of Ventral Tegmental Area Glutamatergic Neurons. J Neurosci 35:15948–15954. https://doi.org/10.1523/JNEUROSCI.3428-15.2015

Warlow SM, Singhal SM, Hollon NG, et al (2024) Mesoaccumbal glutamate neurons drive reward via glutamate release but aversion via dopamine co-release. Neuron 112:488-499.e5. https://doi.org/10.1016/j.neuron.2023.11.002

Wei X, Ma T, Cheng Y, et al (2018) Dopamine D1 or D2 receptor-expressing neurons in the central nervous system. Addiction Biology 23:569–584. https://doi.org/10.1111/adb.12512

Yan Z, Song W-J, Surmeier DJ (1997) D_2 Dopamine Receptors Reduce N-Type Ca^{2+} Currents in Rat Neostriatal Cholinergic Interneurons Through a Membrane-Delimited, Protein-Kinase-C-Insensitive Pathway. Journal of Neurophysiology 77:1003–1015. https://doi.org/10.1152/jn.1997.77.2.1003

Yoo JH, Zell V, Gutierrez-Reed N, et al (2016) Ventral tegmental area glutamate neurons co-release GABA and promote positive reinforcement. Nat Commun 7:13697. https://doi.org/10.1038/ncomms13697

Young EA, Dreumont SE, Cunningham CL (2014) Role of nucleus accumbens dopamine receptor subtypes in the learning and expression of alcohol-seeking behavior. Neurobiology of Learning and Memory 108:28–37. https://doi.org/10.1016/j.nlm.2013.05.004

Zell V, Steinkellner T, Hollon NG, et al (2020) VTA Glutamate Neuron Activity Drives Positive Reinforcement Absent Dopamine Co-release. Neuron 107:864-873.e4. https://doi.org/10.1016/j.neuron.2020.06.011